Robust Nonlinear Output Feedback Control with predefined Bounded States for Fully Actuated Multi-Rotors

Supplementary material

Gerardo Flores, *Member, IEEE*, Almuatazbellah M. Boker, *Member, IEEE*, and Mohammad Al Janaideh, *Member, IEEE*

SIMULATION RESULTS

The system parameters for the simulation are [1]: $J = \text{diag}(0.0820,\ 0.0845,\ 0.1377)\ \text{kgm}^2$, $m = 4.34$ kg, $g = 9.8$ m/s^2. Disturbances $\Delta^v(t)$ and $\Delta^\Omega(t)$ are depicted in Fig. 2.

The parameters of observer (38) are: $\bar{\alpha}_1 = 21$, $\bar{\alpha}_2 = 146$, $\bar{\alpha}_3 = 336$, and $\epsilon_\alpha = 0.01$.

The parameters of attitude controller (32) are: $k_R = 8.81J^{-1}$, $k_\Omega = 2.54J^{-1}$, $\kappa_R = 5J^{-1}$, and $\kappa_\Omega = 0.16J^{-1}$.

The parameters for the output feedback control (39) are: $k_1 = k_2 = k_3 = 30$, and $\beta_1 = \beta_2 = \beta_3 = 50$. While the bounds for the tracking errors are: $l_1 = 0.05$, $l_2 = 0.1$, $l_3 = 0.7$, $m_1 = 0.5$, $m_2 = 1.3$, and $m_3 = 0.8$. They are marked in magenta color in Fig. 4.

All the system's initial conditions are zero except for the rotational matrix, which is $R(0) = R_z(10)R_y(20)R_x(-15)$. The initial conditions for all the observer states are also zero. The position desired trajectory is an elliptical helix: $p^d = (0.4t,\ 0.4\sin(\pi t),\ -0.6\cos(\pi t))^\intercal$ depicted in red color in Fig. 6. Since the UAV is fully-actuated, $R_d = I_{3\times3}$ completes the desired attitude trajectory. Thus, the UAV must track the elliptical helix by maintaining all the attitude angles equal to zero.

Simulation results are presented next. Fig. 1 shows the estimated vectors $\hat{p}$ and $\hat{v}$ vs. their corresponding actual values p and v. While the left-hand side of Fig. 2 depicts the estimated position disturbance $\hat{\Delta}^v(t)$ vs. the actual disturbance $\Delta^v(t)$. Disturbance $\Delta^\Omega(t)$ is shown on the right-hand side of the same figure. Notice that all the time, the system is disturbed, and it is particularly affected during $t = [2.5, 4.5]$ where a peak force of magnitude $\pm 40N$ disturbs the UAV in the y axis.

The attitude e_R and e_Ω in (7) are depicted in Fig. 3, where it is clear its convergence to zero although we do not estimate

Gerardo Flores is with the Laboratorio de Percepción y Robótica (LAPyR), Center for Research in Optics, Loma del Bosque 115, León, Guanajuato, 37150 Mexico (Corresponding author e-mail: gflores@cio.mx).

Almuatazbellah M. Boker is with the Bradley Department of Electrical and Computer Engineering, Virginia Tech, Blacksburg, VA 24060, USA. (e-mail: boker@vt.edu).

Mohammad Al Janaideh is with the Department of Mechanical and Mechatronics Engineering, Memorial University, St. John's, NL A1B 3X5, Canada. (e-mail: maljanaideh@mun.ca).

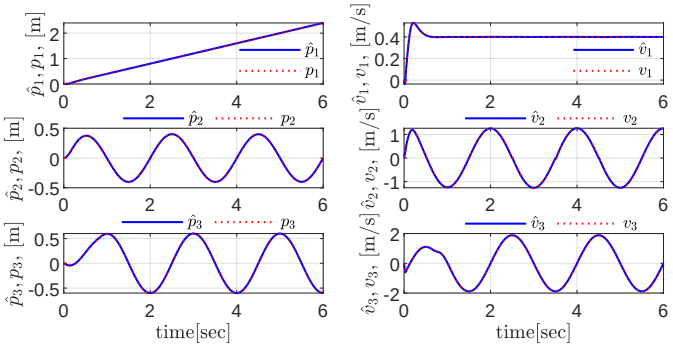

Fig. 1: The convergence of estimated position and velocity states with EHGO (38).

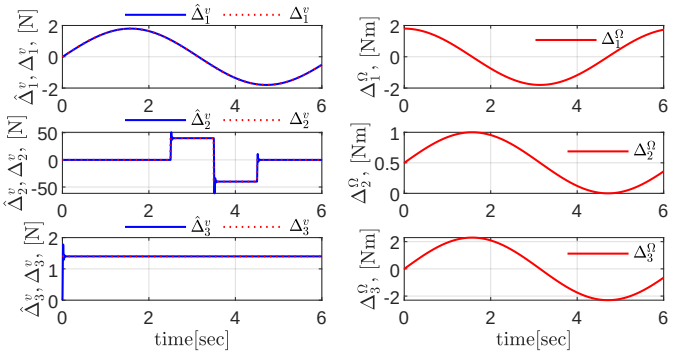

Fig. 2: In the LHS, the position perturbation $\Delta^v(t)$ and its estimate $\hat{\Delta}^v(t)$ with EHGO (38); note the large magnitude aggressive perturbation $\Delta^v_2(t)$. In the RHS, the attitude perturbation $\Delta^\Omega(t)$.

$\Delta^\Omega(t)$; the robust controller (32) perfectly rejects such a disturbance.

Most important is Fig. 4, where the tracking errors (4) are shown together with their corresponding predefined limits l_i for e^p_i, and m_i for e^v_i for all $i = \{1, 2, 3\}$.

Finally, the controls u and u_τ corresponding to (39) and (32), respectively, are shown in Fig. 5. Notice the aggressive response in u_2 during $t = [2.5, 4.5]$ produced to compensate for the undesired effect of $\hat{\Delta}^v(t)$ in the UAV.

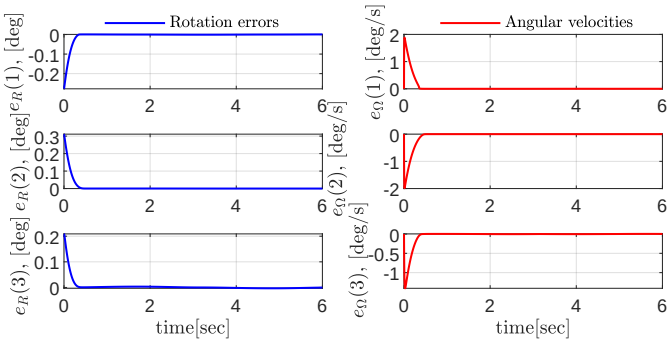

Fig. 3: Convergence of attitude errors e_R and e_Ω to zero.

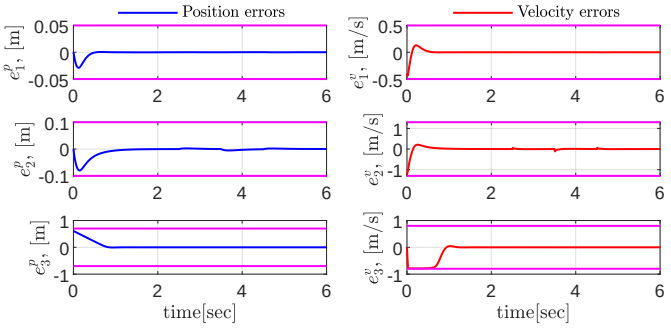

Fig. 4: The user-imposed constraints on the position and velocity error states are in magenta. Notice how the errors respect such bounds; this is especially clear in the first part of e_3^v. The errors rapidly converge with no transient response nor peaks, even in the presence of disturbances.

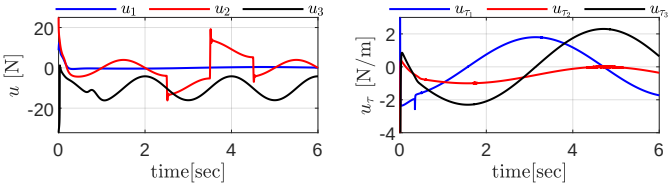

Fig. 5: The proposed controls u and u_τ. During the aggressive disturbance $\Delta_2^v(t)$ shown in Fig. 2, the control term u_2 accordingly responds.

Finally, Fig. 6 shows a 3D plot of the elliptical helix tracking the trajectory of the fully actuated multi-rotor. In addition, the right side of Fig. 6 shows the response of the geometric tracking control in SE(3) presented in [1], which we adapted to control the fully actuated multi-rotor. That controller is famous and has been a reference for many researches and applications. However, despite its high efficiency in most scenarios, our proposed controller outperforms under aggressive perturbations.

REFERENCES

[1] T. Lee, M. Leok, and N. H. McClamroch, "Geometric tracking control of a quadrotor uav on se(3)," in *49th IEEE Conference on Decision and Control (CDC)*, 2010, pp. 5420–5425.

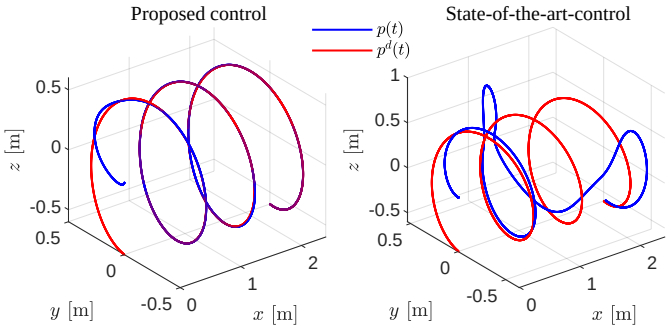

Fig. 6: The desired trajectory of an elliptical helix is in red. In the LHS is the tracking position trajectory using the proposed control. On the RHS, the position trajectory with geometric tracking control on SE(3) presented in [1]. For comparison, we used the same gains as in that work.